Temperature-dependent performance prediction for cerium oxynitride solid-state symmetric supercapacitor using machine learning

Sourav Ghosh, Ashwath Sibi, G. Sudha Priyanga, Zaineb Chelly Dagdia, Tiju Thomas

Temperature-dependent performance prediction for cerium oxynitride solid-state symmetric supercapacitor using Machine Learning

Sourav Ghosh[1,2,*], Ashwath Sibi[2], G. Sudha Priyanga[2,3], Zaineb Chelly Dagdia[4], Tiju Thomas[2,*]

[1]Department of Electronics and Communication Engineering, Saveetha School of Engineering, Saveetha Institute of Medical and Technical Sciences (SIMATS), Chennai, 602105, Tamil Nadu, India

[2]Applied Nanostructures Engineering and Nanochemistry Group, Department of Metallurgical and Materials Engineering, Indian Institute of Technology Madras, Chennai, 600036, Tamil Nadu, India.

[3]Department of Sciences and Methods for Engineering, University of Modena and Reggio Emilia, 42122 Reggio Emilia, Italy.

[4] Université Paris-Saclay, UVSQ, DAVID, France.

*Corresponding author: souravg@alumni.iitm.ac.in (S. Ghosh); tt332@cornell.edu (T. Thomas)

Graphical abstract

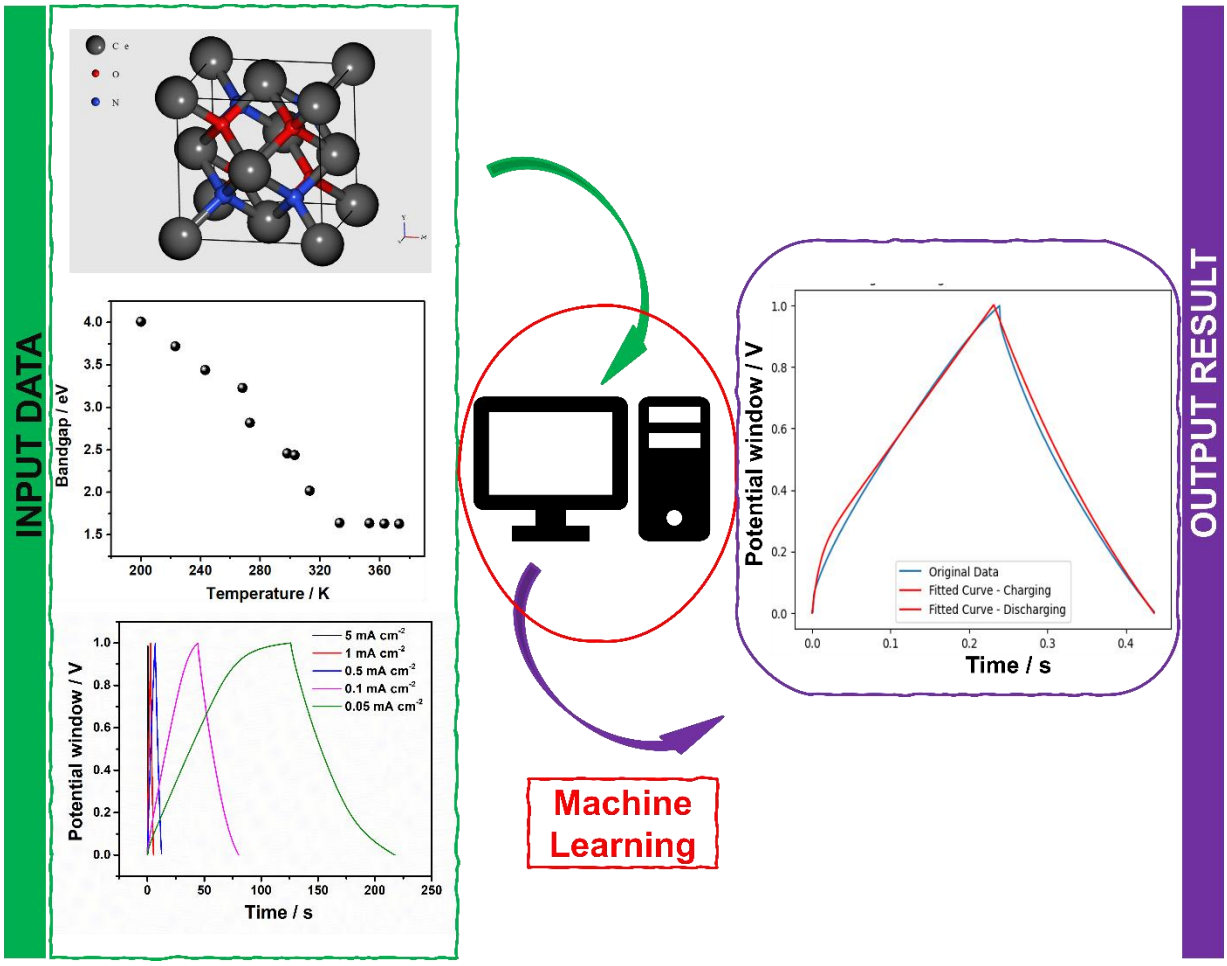

Abstract

The global demand for electricity and dwindling fossil fuel reserves necessitates advanced energy storage solutions like next-generation supercapacitors. This study uses machine learning (ML) to predict the temperature-dependent performance of cerium oxynitride-based solid-state symmetric supercapacitors. Supercapacitors excel in power density and rapid charge-discharge but face challenges under varying temperatures affecting ionic mobility and material stability. Cerium oxynitride, with unique electronic and thermal properties, is analyzed using Density Functional Theory (DFT) to study temperature-induced changes in the Density of States. ML models trained on experimental and DFT data predict charge-discharge behaviour under thermal and current variations. The supercapacitor exhibits good charge storage (~4.6 $mVcm^{-2}$) and low ohmic resistance (~1.6 Ω) at room temperature. The study also models exponential and linear relationships between time and potential window, highlighting the potential of integrating DFT, experimental insights, and ML to tackle temperature variability in supercapacitors.

Keywords: temperature study; machine learning; supercapacitors; oxynitride; energy storage; density functional theory

1. Introduction

The global push for a sustainable future has made energy storage essential in addressing climate change, fossil fuel depletion, and pollution. While renewable energy sources like solar and wind offer cleaner alternatives, their intermittency challenges grid stability, highlighting the need for advanced storage solutions to ensure reliable energy capture, storage, and delivery [1,2]. In this context, energy storage systems, including supercapacitors, batteries, and other emerging technologies, play a pivotal role in enhancing the efficiency and feasibility of renewable energy integration, facilitating a smoother transition to sustainable energy systems[3].

From an environmental perspective, developing efficient energy storage systems is vital for minimizing the carbon footprint associated with energy production and consumption[4]. By enabling more effective utilization of renewable resources, energy storage helps reduce reliance on fossil fuels, lowering carbon dioxide emissions and other harmful pollutants. This transition supports global efforts to meet international climate targets, such as those outlined in the Paris Agreement, which aims to limit global warming to below 2 ^{0}C compared to pre-industrial levels[5]. Energy storage enables decentralized energy systems, empowering local generation and storage, enhancing energy independence, and reducing the environmental impact of long-distance transmission.

Supercapacitors, in particular, have become part of the broader energy storage landscape due to their unique characteristics and ability to bridge the gap between traditional capacitors and batteries[6–8]. Unlike conventional batteries that rely on slow chemical reactions, supercapacitors store energy through electrostatic separation of charges, allowing them to deliver high power density, rapid charge-discharge rates, and superior cycle life with millions of cycles[9,10]. Supercapacitors are ideal for applications requiring quick power bursts, like regenerative braking, backup power, portable electronics, and renewable energy load leveling. However, their lower energy density limits prolonged energy supply. They are classified as electrochemical double-layer capacitors (EDLCs), storing energy via ion adsorption, and pseudocapacitors, utilizing fast redox reactions.[11,12]. A supercapacitor's key components are electrodes for charge storage, electrolytes for ion exchange, separators to prevent short circuits while enabling ion flow, and current collectors connecting electrodes to the circuit. Performance depends largely on electrode materials, which impact capacitance, energy density, power density, and thermal stability. Electrode materials range from carbon-based materials such as activated

carbon, graphene, and carbon nanotubes, known for their high surface area and excellent conductivity, to transition metal oxides (e.g., RuO_2, MnO_2, NiO, $CoFe_2O_4$), conducting polymers (e.g., polyaniline, polypyrrole), nitrides (e.g., TiN, VN), etc[13–17]. Novel materials like oxynitrides, MOF-derived materials, bimetallic chalcogenides, etc, have been explored recently in a similar context. These materials are studied to improve charge storage and optimize energy and power density. Density Functional Theory (DFT) provides a theoretical framework to analyze atomic-level interactions, including the Density of States (DOS), which influences electrochemical performance. Elevated temperatures can shift the DOS, altering conductivity, ion adsorption, and reaction kinetics, impacting charge storage capacity and cycling stability.

For instance, Yu-Ning Wu *et al* investigated the temperature effects on the band gap and optical properties of rutile TiO_2 using ab initio methods[18]. They found that electron-phonon interactions are the main factor affecting band gap changes with temperature, leading to a band gap narrowing by about 138 meV at 1000 K. The findings also align with experimental data on refractive index and dielectric constants, offering insights for developing high-temperature materials for optical gas sensing applications. On the other hand, the temperature-dependent DFT studies have been carried out by Ashish et al.) on VS_2 electrodes, and they found that doping VS_2 electrodes with non-metallic elements like nitrogen, phosphorus, and arsenic enhances their quantum capacitance[19]. Among them, As-doped VS_2 exhibited the highest quantum capacitance and maintained a stable capacitance at higher temperatures. Additionally, the band structure of the doped VS_2 monolayers showed metallic properties, making them promising for supercapacitor electrodes, with As-doped VS_2 achieving a high figure of merit due to its excellent electrical conductivity. Bharti et al studied the density of states and quantum capacitance of pure and cobalt-doped niobium nitrides using DFT[20]. NbN shows high quantum

capacitance, making it a strong candidate for supercapacitor electrodes. Cobalt doping further enhances this property, and both pristine and doped niobium nitrides outperform graphene regarding quantum capacitance near the Fermi level.

Temperature significantly affects supercapacitors, impacting ionic mobility, conductivity, interface stability, and efficiency. Low temperatures hinder ion transport, reducing capacitance, while high temperatures improve conductivity but risk material degradation, shorter cycle life, and thermal runaway.[21–24]. Studying temperature-dependent supercapacitor performance is vital for applications in extreme thermal environments, like automotive or aerospace. It aids in designing resilient materials and systems for reliable, safe, and optimal performance under varying conditions.

Machine learning (ML) is used here for temperature-dependent performance evaluation, offering a powerful tool for analyzing data, identifying patterns, and making predictions. ML aids in material property prediction, synthesis optimization, performance forecasting, and discovering advanced materials for supercapacitors [25–29]. ML algorithms can be trained using experimental measurements, DFT simulations, and electrochemical testing data to predict key performance metrics such as capacitance, energy density, cycle stability, and thermal behaviour [30–34]. Different data-driven algorithms used for different electrochemical energy storage systems are tabulated in Table S1 for further study.

This work uses ML to predict supercapacitor performance at high temperatures, offering insights into thermal resilience, optimizing materials, and identifying degradation pathways for better performance in harsh environments.ML has been used in the literature to predict temperature-

related predictions for different photovoltaics applications and for air temperature inside buildings[37,38].

This paper uses machine learning to predict the temperature-dependent performance of cerium oxynitride-based solid-state symmetric supercapacitors, chosen for its high conductivity, thermal stability, and unique electronic structure. It explores how ML models, trained on experimental and DFT data, can predict the charge-discharge behavior of cerium oxynitride electrodes across various temperatures. Integrating ML with DFT insights allows for a comprehensive understanding of how electronic properties such as DOS evolve with temperature, directly impacting the supercapacitor's performance[39–41]. By modelling these temperature-dependent changes, this work provides a predictive framework that can be extended to other advanced materials, driving the design of next-generation supercapacitors with improved thermal performance.

2. **Experimental and Computational Methodology**

2.1. Materials

The supplementary material file provides the detailed materials synthesis process and corresponding XRD and Scanning electron microscopy images. Further details are provided in the literature [42,43]. The detailed device fabrication process is provided in the section below.

2.2. Electrode and device preparation

This active material is CeO_XN_Y, and it is used to prepare the slurry along with acetylene black and PVDF in a ratio of 85:10:5 in NMP solvent. Ni foam is the current collecting substrate on which the active material is coated. The coated Ni foam is used to create a circular electrode of

18mm diameter with a 2 mg cm^{-2} mass loading of the mixed active material. The Ni foam is kept in the heating oven at 80 ^{0}C (8 h duration) for drying.

Processing of the Ni foam before using it as the current collecting substrate: Washing of the Ni foam is done in three continuous steps – (i) *step 1:* foams are dipped into 3 M HCl solution and washed, (b) *step 2:* next DI water is used as the washing agent, and then (c) *step 3:* finally, ethanol is used to wash the foam electrodes. Rigorous washing is crucial to remove the oxide layer on the surface of the electrodes. After three step washing is completed, the foams are kept at 60 ^{0}C for 6 h. This process will help dry the foams and make them ready for the coating process mentioned above.

The solid-state symmetric supercapacitor is fabricated in a CR2032 coin cell. The coin cell is studied for this work, and all the data are collected based on the two-electrode study using the fabricated coin cell. The symmetric device contains CeO_XN_Y-based slurry coated on the Ni foam, used as both positive and negative electrodes (hence the term "symmetric" is used). PVA-KOH-based gel electrolyte (prepared with 2 M KOH) is used along with a separator of cellulose filter paper.

2.2. Electrochemical characterization and relevant formulas

Post fabrication, the device's electrochemical performance is observed using the CHI608E electrochemical workstation. The electrochemical studies are carried out in a potential window of 0 to 1 V. The study on temperature variations is done in the Weiss environmental-climate chamber. The temperature is increased stepwise from 10 to 70 ^{0}C with a step size of 10 ^{0}C. The humidity inside the chamber is kept fixed at 50 % relative humidity (RH). The fabricated supercapacitor device is housed inside the environmental chamber for 24 h duration to confirm

that the whole device is at the same temperature. This process ensured the reliability of the data acquisition during the temperature-dependent electrochemical study. Conventional electrochemical studies for supercapacitors, such as cyclic voltammetry analysis, electrochemical analysis, and galvanostatic charge-discharge process, are done at room temperature. The charge-discharge studies are done in different temperatures to aid the data-driven study on the charge-discharge prediction at higher temperatures. The areal capacitance (AC) is calculated using the equation given below:

$$AC=\frac{\int_{V1}^{V2} I_s \times V dV}{ESA \times \nu \times (V2-V1)} \qquad (1)$$

In equation (1), 'V2' is upper limit of the potential window and 'V1' is the lower limit of the potential window. Here the value of 'V2 – V1' is equal to 1 V. The scan rate is denoted with 'ν' and the unit is mVs^{-1}. ESA stands for electrode surface area. The 'I_S' signifies the current value per area with a unit of $mAcm^{-2}$. The areal capacitance using a charge-discharge plot at a constant current value (AC_G) is calculated using the equation below:

$$AC_G=(I_S \times t_{dis})/(ESA \times (V2-V1)) \qquad (2)$$

The t_{dis} stands for the discharge time in the galvanostatic charge-discharge plot.

2.3. Density Functional Theory

The DFT tool of the Vienna ab initio simulation package (VASP) is used to analyse the structural and electronic properties of CeO_XN_Y with projector-augmented wave (PAW) potentials along with a plane-wave basis set of cutoff energy of 460 eV[44,45]. The generalized gradient approximation (GGA-PBE) developed by the Perdew–Burke–Ernzerhof is used as exchange and correlation potential[46]. An 11x11x11 Monkhorst Pack k-point mesh is used for the Brillouin

zone scheme[47]. Along with the periodic boundary state, the spin-polarized calculation is also performed. In this work, the calculations are designed to optimise the lattice constant of CeO_XN_Y concerning total energy calculations for various temperatures. A stable configuration of the CeO_XN_Y compound upon temperature can be found by integrating the lattice distortion and the thermal expansion of Ce/O(N) ions from equilibrium positions, even though the ab initio calculations have been performed at 0K. This study has successfully predicted the electronic structure of CeO_XN_Y for the temperature range from 268 K to 353K using the above technique.

2.4. Details of the Database

A database is compiled using SCC experimental data under different temperatures. The database contains features such as: a) Current (A), b) Temperature (^{0}C), c) Bandgap (eV), d) Time (s), and e) Voltage (V). The range of temperature considered for this work is 10 - 70 °C. The galvanostatic charge-discharge data are collected against various current values ranging from 1 mA to 20 mA. Bandgap is a critical feature that determines the mobility of charge carriers between the anode and cathode during charging and discharging. Also, the bandgap directly depends on the temperature (a detailed computational study regarding band gap and temperature is provided in section 3.1), where the experimentation is conducted. This is because, with increased temperature, materials undergo expansion, resulting in changes in lattice parameters and interatomic distances. This can influence the electronic structure of the materials, thus affecting the bandgap.

Due to the relation of bandgap and temperature, the concern of multicollinearity arises. Multicollinearity is a statistical phenomenon in regression analysis where two or more independent variables in a model are highly correlated. In simpler terms, it means that there is a

linear relationship between two or more predictor variables. This correlation among independent variables can pose challenges in estimating the individual coefficients and understanding the true relationships between the independent and dependent variables. Multicollinearity becomes a concern when these relationships are too strong. In this work, bandgap and temperature share a correlation value of 1.0. To avoid multicollinearity, only temperature was fed into the model. The objective was to predict the voltage curve for 70 °C, with temperatures up to 60 °C as the training dataset.

2.5. ML Algorithms

Decision Trees and Random Forests are popular ML algorithms in supercapacitor research, helping with performance prediction, material discovery, and optimization. Decision Trees split data into branches based on input features, offering precise, easy-to-understand models showing how material properties or operating conditions impact performance. This makes them especially useful for predicting electrode performance under different temperatures or classifying materials by electrochemical properties. However, Decision Trees can sometimes overfit noisy data, making them less reliable for new datasets[48–50]. Random Forests tackle overfitting by combining multiple decision trees and averaging their predictions, resulting in more accurate and reliable models. This makes them ideal for capturing the complex, non-linear behavior of supercapacitors. However, they are less interpretable than single decision trees and can be computationally demanding, requiring more processing power and memory[51]. Decision trees and random forests are potent tools for advancing supercapacitor research and balancing interpretability, robustness, and computational efficiency. This work also utilizes support vector regression and linear regression.

3. Results and Discussions

3.1. DFT analysis

The electronic properties need to be controlled as decisively as possible to accomplish superb execution of the materials for modern applications, especially oxides and oxynitrides. In this way, it is crucial to know precisely the reliance of the energy bandgap of oxides and oxynitrides on the arrangement and temperature. Numerous studies have shown that as the temperature rises, the energy gaps of oxides and oxynitrides decrease [52]. This temperature dependence is very close to that seen in crystals and is generally explained by thermal lattice expansion and electron-phonon interactions [53]. On the other hand, from an atomistic standpoint, little is known about the mechanism underlying the temperature dependence of the energy gaps of the materials mentioned above. Consequently, it is critical to explain this component, considering the structural fluctuation expected to increase as miniaturization progresses. Due to the high computational costs involved, mainly when first-principles methods are used, few electronic structure calculations have been performed on the temperature dependence of energy gaps.

The lattice parameter of CeO_XN_Y increases monotonically as the temperature rises, as seen in graph X. By comparing the value at 353 K to the value at 0 K, it is observed that the thermal expansion along an x-axis increases by 0.6 per cent. The band gap variance contributed by lattice thermal expansion can be determined using the corresponding lattice constants, as shown in Fig. 1. The bandgap shift indicates a gradual decrease from 0 to 200K, then a steady behaviour for temperatures above 200 K. Compared to 0 K, the band gap is reduced by 1.18 eV at 333K. Like numerous different semiconductors, the fundamental computational estimations on CeO_XN_Y show comparable patterns of band gap narrowing with expanding temperature[54].

The total and partial density of states (DOS) were computed to analyze the electronic properties of CeO_XN_Y at different temperatures. The outcomes are shown in **Figure 1**. The dotted flat line indicates the Fermi energy level (E_F). **Figure 1** shows that the CeO_XN_Y is a wide band gap semiconductor (E_g= 2.82 eV) at 0 ^oC. The N-2s and N-2p peaks are sharp and narrow, which lie in the range of ~-18 eV. These are very different from the peaks near the Fermi level, dominated by O-2p states, found near ~-10 eV. The peaks form below E_F due to O-2p and N-2p state electrons and a relatively minor contribution from Ce-5d state electrons. Above E_F, there is a hybridization between Ce-4f and the O-2p states. The highest peaks in the conduction state of CeO_XN_Y are due to Ce-4f, with a minor contribution from Ce-5d and O-2p state electrons [**Figure 1**].

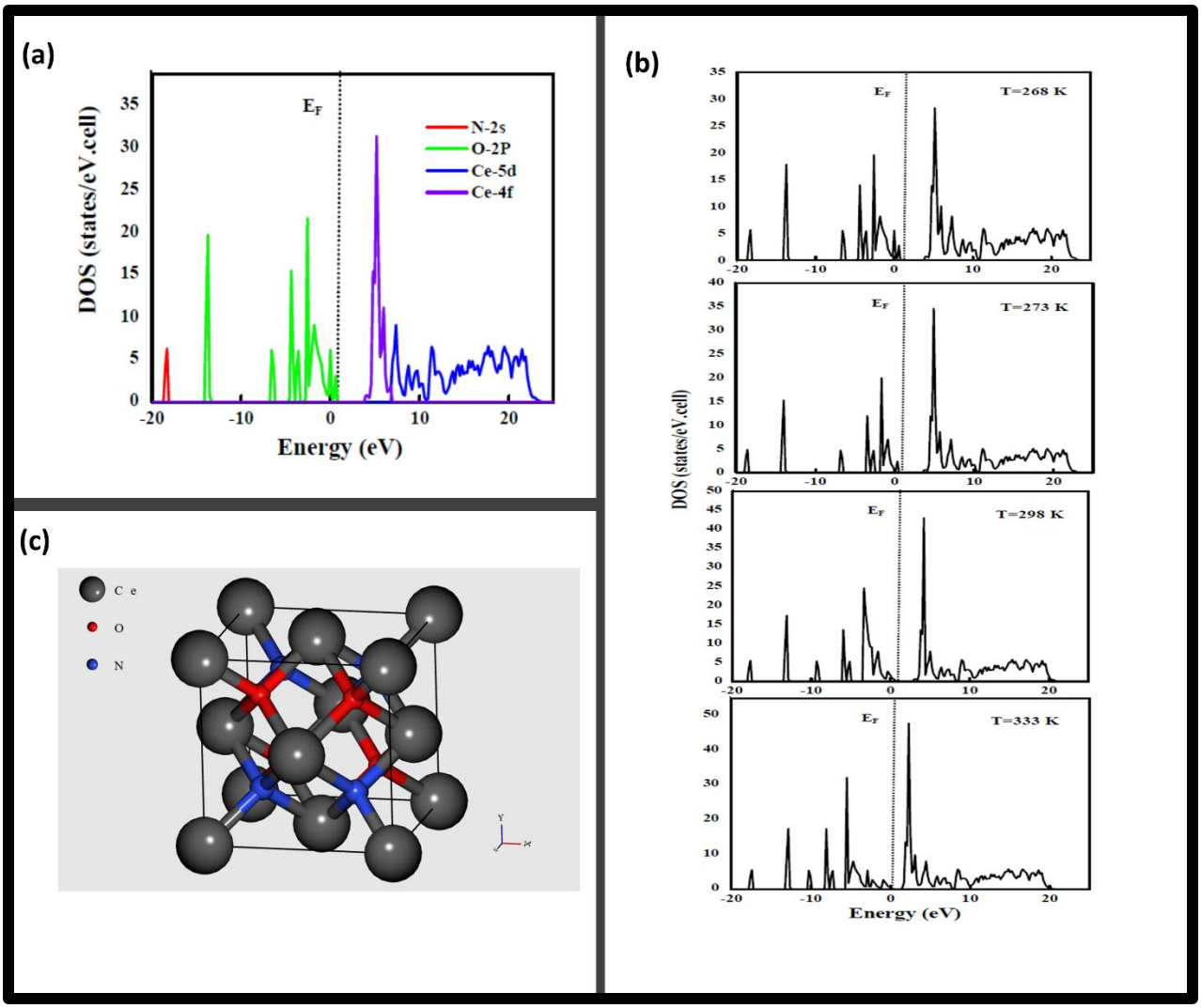

269

270 **Figure 1.** (a) The partial density of states (PDOS) of CeO_XN_Y (b) the total density of states of
271 CeO_XN_Y at different temperatures, (c) the crystal structure of CeO_XN_Y. Fermi energy and band
272 gap decrease upon reducing temperature.

273 The DOS of CeO_XN_Y shows a significant change in the conduction state because of the
274 expansion in temperature. The Fermi level of CeO_XN_Y also decreases and shifts downwards from
275 0 ^oC, as shown in **Figure 1**. With rising temperature, the lattice expands, increasing the
276 interatomic distances. This reduces the overlap of atomic orbitals, which decreases the band
277 dispersion and shifts electronic states to lower energy. Moreover, the hybridization strength,

particularly between Ce-4f and O-2p states in CeO_XN_Y, weakens, reducing the conduction band's width and lowering the Fermi level. The dependence of the electronic structure on thermal lattice expansion has been studied in oxide materials by Lucovsky et al. [55], and they discussed how thermal expansion leads to electronic band shifts in transition metal oxides, which correlates with the findings here. Additionally, increased temperatures may enhance lattice vibrations (phonons), which interact with electronic states and redistribute energy levels. This interaction causes a shift of electronic states to lower energy regions. It narrows the effective bandgap, as observed in oxides and semiconductors like Si and GaAs, as reported by Zollner et al. [56]. These mechanisms extend to wide bandgap materials such as oxides and oxynitrides and agree with the results in this work. Furthermore, the narrowing of the peaks occurs because thermal vibrations introduce disorder into the system. This reduces the coherence of the electronic states, leading to a less uniform distribution of states and sharper, narrower peaks at specific energy levels. Theoretical studies by Giustino et al. [57] on the electron-phonon coupling in semiconductors align with this observation. They demonstrate that thermal disorder reduces the density of available states, leading to more localized features. Thermal expansion and phonon interactions explain the temperature-dependent shifts and narrowing of DOS peaks observed in materials like CeO_XN_Y.

As a result of the increased temperature, the width of the conduction state in CeO_XN_Y is reduced, and the height of the peak is increased. The decrease in the band gap is primarily due to a change in the conduction state and a decrease in the Fermi level value, which predominantly comes from the relatively minor hybridisation between Ce-4f and O-2p state electrons. The relation between lattice constant, Fermi level (E_F), and bandgap is provided in Table 1. The experimental relevant outcomes are the following - (i) Lattice parameters increase with temperature rise, (ii) Fermi

energy and band gap decrease upon reducing temperature, (iii) Peaks are shifted towards the lower energy region and narrowing, (iv) The highest peak is due to Ce-4f state orbital with little contribution from O and N-2p states (indicates the hybridisation), and (v) The majority peaks in the valence and conduction bands are due to O-2p and Ce-5d states, respectively.

Table 1: Relation between temperature, Lattice constant, Fermi Level and Bandgap of CeO_XN_Y.

T (K)	Lattice constant	E_F (eV)	Eg (eV)
200	5.249	1.510	4.01
223	5.286	1.466	3.72
243	5.301	1.379	3.44
268	5.360	1.366	3.23
273	5.401	1.101	2.82
298	5.416	0.799	2.46
303	5.420	0.710	2.44
313	5.424	0.502	2.020
333	5.428	0.120	1.642
353	5.431	0.118	1.638
363	5.439	0.116	1.634
373	5.442	0.112	1.630

3.2. Analysis of Electrochemical Characterization

The electrochemical properties of the symmetric coin cell (SCC) are evaluated using cyclic voltammetry (CV), galvanostatic charge-discharge (GCD), and electrochemical impedance spectroscopy (EIS). As depicted in **Figure 2a**, the CV profiles for SCC exhibit a quasi-rectangular shape characteristic of typical pseudocapacitor behaviour within a potential range of

0 to 1 V at a scan rate of 10 to 100 mVs^{-1}. These electrodes' overall working potential windows define the device's effective cell voltage, resulting in a symmetric solid-state supercapacitor with a cell voltage of 1 V.

The CV curves for the SCC device is studied at a 10 to 100 mV/s scan rate range. The curves exhibit characteristics typical of pseudocapacitors with quasi-rectangular shapes[58,59]. The SCC device demonstrates an areal capacitance of 4.11 mF cm^{-2} at a scan rate of 10 mV s^{-1} and 2.91 mF cm^{-2} at 100 mV s^{-1}. Notably, it retains ~70.8% of its initial capacitance at higher scan rates, indicating robust rate capability even under rapid scanning conditions. The reduced charge storage capability in higher scan rates is a well-documented phenomenon in supercapacitor devices, primarily due to less interaction of electrolyte ions with the active electrode materials[60,61]. Typical governing equations for the CV study is added in the supplementary file.

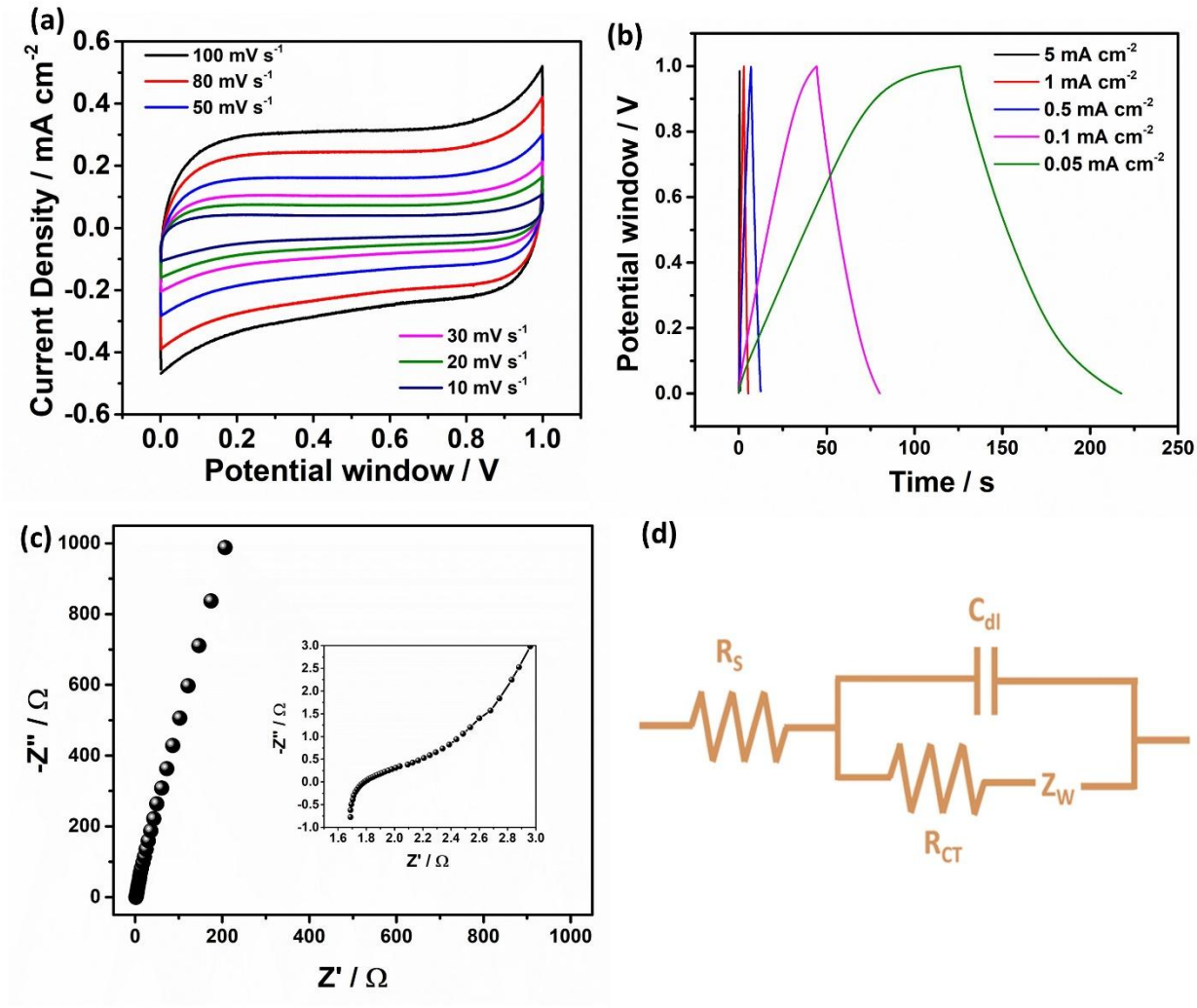

Figure 2. Electrochemical characterization study conducted at room temperature of the symmetric coin cell fabricated using the cerium oxynitride electrode. (a) cyclic voltammetry study for various scan rates, (b) charge-discharge plot at constant current at various current densities, (c) Nyquist plot derived from electrochemical impedance spectroscopy study, and (d) representative equivalent circuit of the device using the series resistance (R_s), charge-transfer resistance (R_{CT}), double layer capacitance (C_{dl}), and Warburg impedance (W).

The GCD curves of the SCC device at a current density range of 0.05 to 5 mA cm^{-2}, are

illustrated in **Figure 2b**. The curves exhibit a characteristic triangular shape, indicative of symmetric supercapacitor behaviour. The device achieves a maximum areal capacitance of ~4.6 mF cm^{-2} at a current density of 0.05 mA cm^{-2}. In **Figure 2c**, the Nyquist plot of the SCC device is displayed over a frequency range from 0.01 Hz to 100 kHz. The inset highlights a depressed semicircle in the high-frequency region, followed by a linear segment in the low-frequency region, corresponding to charge transfer and diffusion resistance, respectively. The depressed semicircle suggests the presence of interfacial charge-transfer resistance, while the transition between the semicircle and the linear portion indicates diffusion-controlled processes. The linear region reflects the capacitive nature of the device. This demonstrates that the SCC device utilizes three distinct charge storage mechanisms: (a) interfacial surface redox reactions, (b) diffusion-controlled processes, and (c) capacitive charge storage[62–64]. The coin cell shows a solution resistance (ESR) of ~1.6 Ω. Figure 2d shows the representative equivalent circuit of the device based on the electrochemical impedance spectroscopy. The low series resistance value highlights the oxynitride-based device's rapid kinetics and excellent rate capability, contributing to its high cyclic stability.

3.3. Machine Learning-based Study

This work deals with the effect of temperature on the charging-discharging of the coin cell. With increasing temperature, faster charging is observed, and it also agrees with the literature. From the work of Jiao-ling Hong et al., it is shown that the increased temperatures lead to a reduction

in electrolyte viscosity resistance. This facilitates accelerated ion movement and diffusion within the supercapacitor. This enhanced mobility enables a greater influx of ions into the porous electrode, resulting in the supercapacitor's expanded capacitive storage capacity. This increase in ion mobility helps increase current flow while charging and improves performance at higher temperatures.

This work uses Decision Trees and Random Forests for regression tasks. Decision Trees predict continuous values by splitting data into decision nodes based on features, creating a simple, interpretable tree structure that captures both linear and non-linear relationships. Random Forest, an ensemble method, builds multiple decision trees using random subsets of data and features, then averages their outputs for a robust prediction. Chosen for its ability to handle non-linear relationships and mitigate overfitting, Random Forest is particularly suited to experimental data, where noise can obscure underlying patterns. Additionally, linear regression and support vector machines were also tested. Linear regression assumes a linear relationship between variables, while support vector machines find an optimal hyperplane to separate or fit data with maximum margin in a high-dimensional space. This work aims to predict SCC charge storage performance at higher temperatures using lower-temperature electrochemical data. The step-by-step procedures and data-driven insights are outlined below.

From the charge-discharge plots of the supercapacitor, observations indicate that the time period for each charge-discharge cycle increases with an escalation in temperature and decreases with a fall in the current value (**Figure 3**). Hence, the initial step is to address this pattern to predict the time period for a temperature of 70 ^{0}C at various current values. A new feature (or variable), named 'Time period', is introduced to calculate the total time for a specific temperature and current. **Fig. 3** demonstrates a proportionality-based relation between the time period and

temperature. On the other hand, the time period is observed to decrease with the current, particularly in the logarithmic scale. This is a known phenomenon in energy storage materials examined under different constant current values for charge-discharge analysis.

Subsequently, machine learning algorithms such as linear regression, support vector regression, decision tree and random forests are constructed with temperature and current as independent variables and time period as the dependent variable. For decision trees and random forests, temperature and current are treated as input features. The ratio of temperature and current is considered the input feature for linear regression and support vector regressors with linear kernels. This is done because linear kernels are suitable for linear regression and support vector regression algorithms due to their computational efficiency and performance for linear relationships. Their effect becomes optimum when data can be separated by a plane, hyperplane, or a straight line. In support of this opted methodology, a work by Nariswari et al. can be referred to, where it is observed that the support vector machine with a linear kernel outperforms other models while evaluating non-linear data[65]. The machine learning models underwent training and arranged along with their mean squared error values in Table 2.

Table 2: Comparison of different Machine learning models in terms of mean squared error.

Machine learning algorithm	Mean squared error
Linear regression	0.48
Support vector regression	4.80

Decision tree	0.06
Random forest	7.02

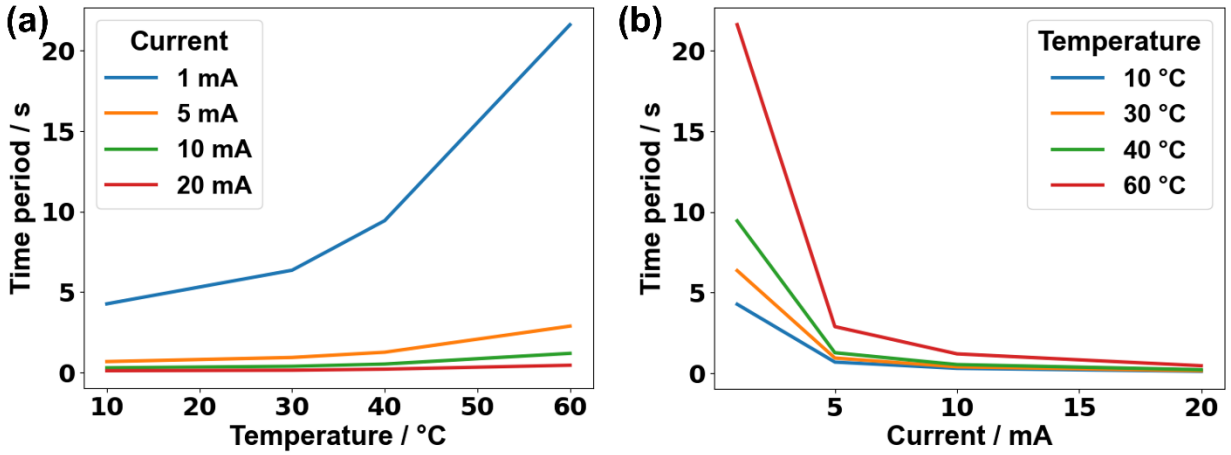

Figure 3. Variation of time period with temperature and current. (a) depicts an increasing time period with rising temperature at different current values and (b) a decreasing time period with increasing current values at different temperatures.

The decision tree performed much better than the other models, as shown in Table 2. Further, to optimize the model's performance, hyperparameter tuning is conducted on parameters such as 'max_depth', 'min_samples_split', and 'criterion'. 'max_depth' represents the maximum depth of the tree. It controls the maximum number of levels from the root node to the deepest leaf node. 'min_samples_split' is the minimum number of samples required to split an internal node. If the number of samples at a node is below this threshold, the node will not split, becoming a leaf node. The 'criterion' parameter determines the function used to measure the quality of a split. This tuning is accomplished through GridSearchCV, a technique for hyperparameter optimization in machine learning[66]. GridSearchCV, part of the scikit-learn library in Python,

executes an exhaustive search over a specified parameter grid to identify the best combination of hyperparameter values for a given model. GridSearchCV also helps avoid overfitting, as it performs cross-validation, up to 5 iterations, on each combination. The resulting model exhibited exceptional performance, achieving an R^2 score of 99.92% and a mean squared error of 0.05. The R^2 score, also known as the coefficient of determination, is a statistical metric illustrating the proportion of the variance in the dependent variable explained by the independent variables in a regression model. The formula for the R^2 score is defined as:

$$R^2 = 1 - \frac{Sum\ of\ squared\ residuals}{Total\ sum\ of\ squares} \quad (3)$$

Table 3: Performance of the model to predict the time period at 70 ^{o}C.

Current (mA)	Calculated time period (s)	Predicted time period (s)	Difference (%)
1	23.26	21.60	7.13
5	3.04	2.89	4.93
10	1.22	1.20	1.63
20	0.48	0.46	4.16

Table 3 shows that the predicted time period value is considerably close to the calculated value, with a maximum difference of ~7.1 % and a minimum difference of ~1.6%. This low difference highlights the ML model's good performance in predicting the time period. The next task is to plot the charge and discharge cycle and observe the visible difference in the alignment of the charge-discharge plots. Therefore, the subsequent objective involved the construction of the

charge-discharge cycle utilizing the calculated and predicted time periods. The temperature dependency (with fixed current value) and current dependency (with fixed temperature value) are given in **Figure 4**.

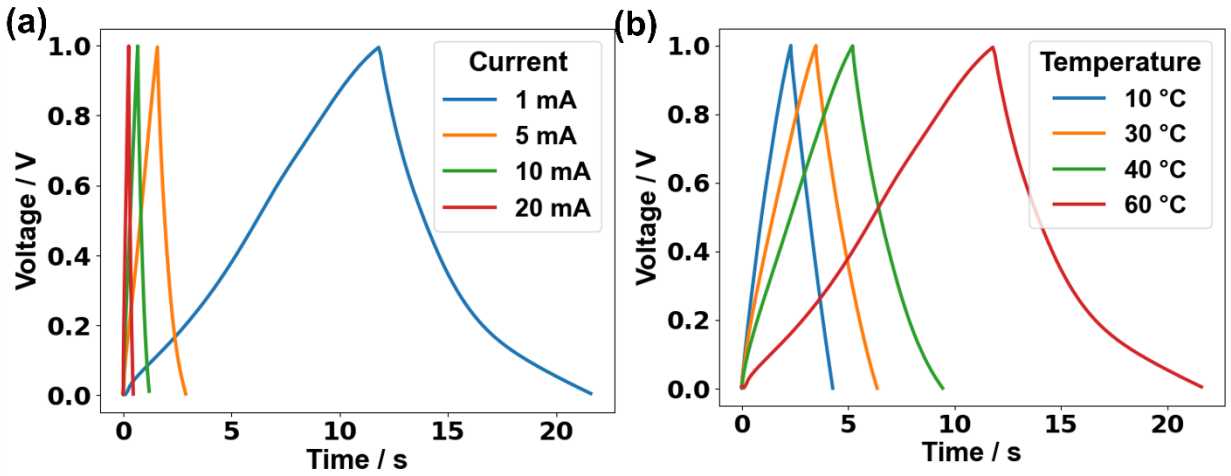

Figure 4. Galvanostatic charge-discharge curves for (a) different current values at a fixed temperature of 60 ^{0}C and (b) different temperatures at a fixed current value of 1 mA.

The voltage-time curve exhibited both exponential and linear behaviours. Furthermore, observations revealed that variations in temperature and current influenced the curve's behaviour, with an increase in temperature and decrease in current leading to a more exponential response, and conversely, a decrease in temperature and increase in current resulting in a more linear behaviour. As a result, the voltage is conceptualised as a function of time, integrating both exponential and each term. The formulation for charging looks as follows:

$$V(t) = b \times (1 - e^{-\frac{t}{a}}) + c \times t \quad (4)$$

The formulation for discharging looks as follows:

$$V(t) = b \times (e^{-\frac{t}{a}}) + c \times t \quad (5)$$

The parameters ‘a’, ‘b’, and ‘c’ in both equations underwent optimization and tuning. The devised function is specifically designed to align with the existing time and voltage data for each time period, employing a maximum of 25,000 iterations. The parameters exhibited variations in response to temperature, and the formulated functions aimed to capture these bi-natured variations (linear and exponential). The variation of the parameters with temperature is depicted in **Figure 5** for the charging and discharging scenario.

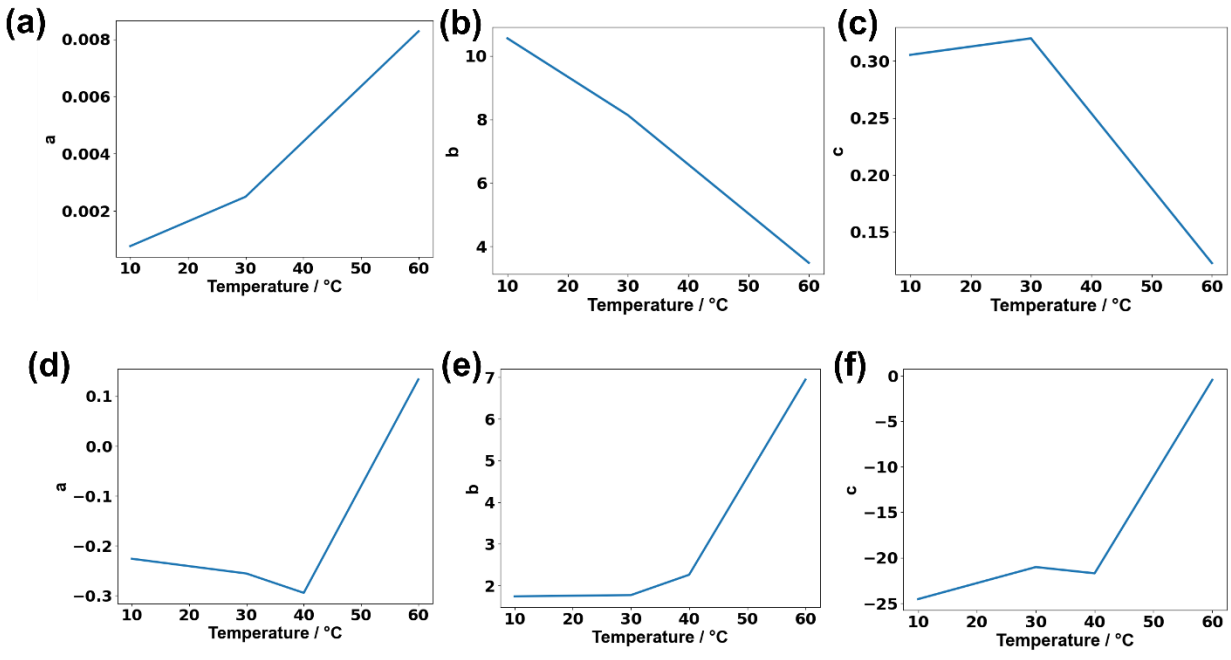

Figure 5. Variation of ‘a’, ‘b’, and ‘c’ parameters against increasing temperature at a constant current value while charging for (a) parameter ‘a’, (b) parameter ‘b’, (c) parameter ‘c’, and while discharging for (d) parameter ‘a’, (e) parameter ‘b’, (f) parameter ‘c’.

Subsequently, distinct Random Forest models were constructed, each with different parameters mentioned above as the dependent variable and the time period as the independent variable. Analogous to the earlier prediction of the time period, these models underwent training with time periods associated with temperatures up to 60 °C. Subsequently, they are utilized to forecast time

periods for a temperature of 70 °C. This iterative process is replicated for both the charging and discharging segments of the cycle. The predicted parameters were then employed to formulate the voltage function plotted against time. The experimental data is confined to charging up to 1V (this is due to the electrochemical potential window of 1 V as discussed in section 3.2), so the predicted function is appropriately scaled before visualization. The comparative performance of the predicted and original curves is demonstrated below (**Figure 6**).

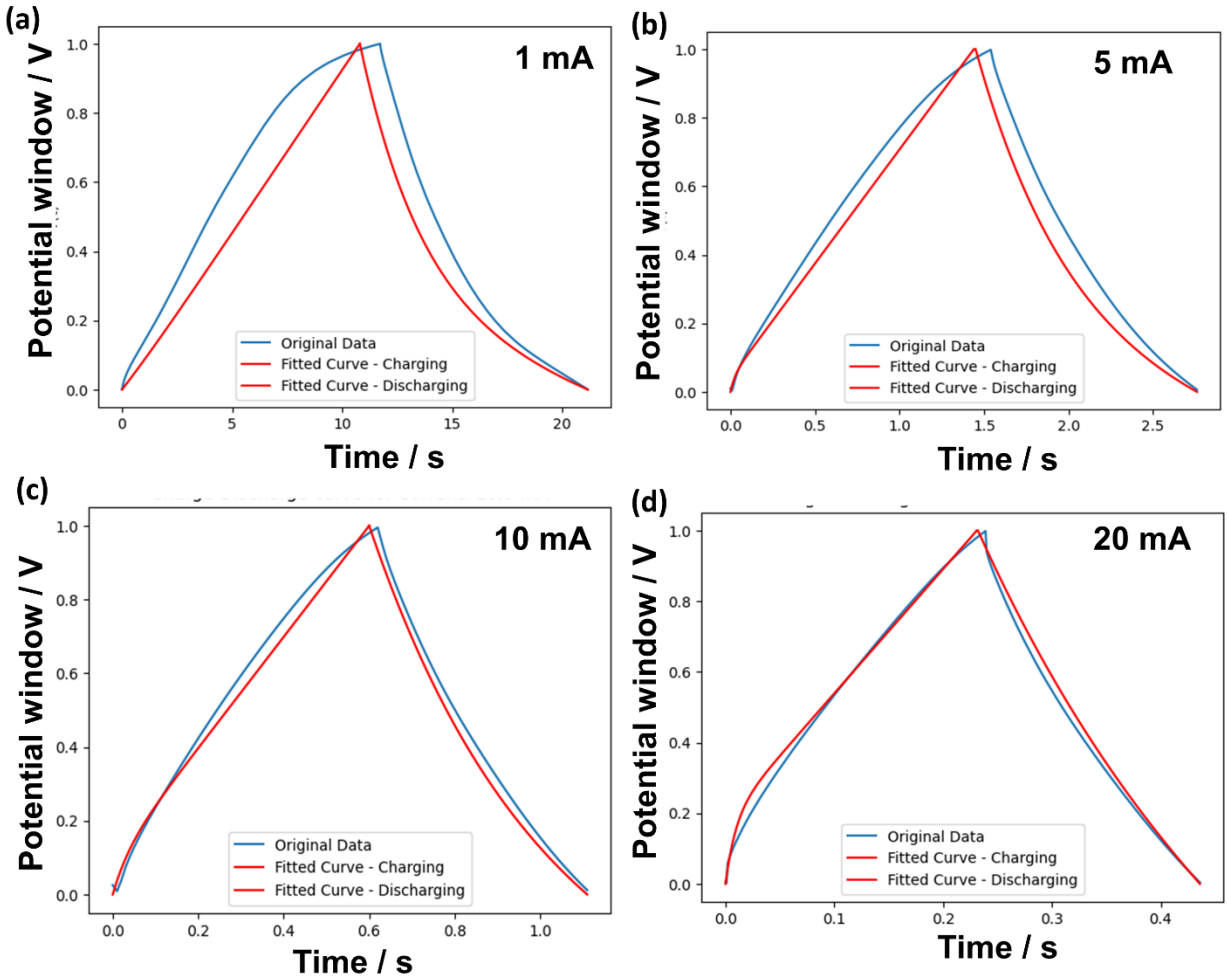

Figure 6. Machine learning derived predicted galvanostatic charge-discharge curve at 70 ^{0}C for different current values, (a) 1 mA, (b) 5 mA, (c) 10 mA, and (d) 20 mA.

This ML-based study demonstrates the potential to predict supercapacitors' high-temperature charge storage performance using lower-temperature electrochemical data. Heating, caused by internal resistance during high-frequency charge-discharge cycles, impacts supercapacitor performance in buffer circuits, leading to efficiency loss and potential electrode and electrolyte damage. Hence, predicting the charge-storage performance of the supercapacitor electrode materials at a higher temperature bears contemporary importance in advanced energy storage solutions [67–69].

The ML model developed in this study accurately predicts supercapacitor performance across varying temperatures, aiding material and device optimization under operational conditions. These insights are crucial for scaling the technology, identifying temperature limits, performance bottlenecks, and energy-efficiency trade-offs, and supporting prototype testing (TRL 6) and system integration (TRL 7). Cerium oxynitride shows promise as an electrode material, with future work on large-scale synthesis and real-world testing poised to advance it to higher TRLs.

4. Conclusion

This work focuses on the application of ML in the temperature-dependent performance of supercapacitors. Combining machine learning with DFT insights, this article provides a comprehensive approach to optimizing thermal resilience in supercapacitor electrodes. Cerium oxynitride offers a reasonable charge storage capability of ~4.6 mF cm^{-2} and low ohmic resistance of ~1.6 Ω in a symmetric coin cell setup. Consequently, the temperature-dependent data are taken by running electrochemical tests inside an environmental chamber by increasing the temperature stepwise. Finally, the Random Forest algorithm is used to predict the charge-discharge performance at higher temperatures and different applied current values (1 to 20 mA). Data-driven study is utilized to model to capture both exponential and linear relation of the

potential window with respect to time, during both charging and discharging. The value of the relevant parameters associated with time and potential window is iterated over 25,000 times before finalizing the model.

Energy storage is vital to achieving a sustainable and resilient energy future. Advancing this field requires integrating high-performance materials with data-driven predictive models to overcome limitations and unlock potential. This work underscores the transformative impact of combining data-driven methodologies with electrochemistry and materials science, paving the way for innovative strategies essential for a greener future.

Acknowledgements

T. Thomas acknowledges support from Anusandhan National Research Foundation and SERB, DST, for the research work. S. Ghosh, G. S. Priyanga, and T. Thomas are grateful to the Department of Metallurgical and Materials Engineering, IITM. Zaineb C.D. acknowledged DAVID, UVSQ. S. Ghosh acknowledges SIMATS for this work.

Data Availability

Data can be obtained upon request from the corresponding author.

Declaration of Competing Interest

The authors declare that they have no known competing financial interests or personal relationships that could have appeared to influence the work reported in this paper.

References

[1] T.R. Ayodele, A.S.O. Ogunjuyigbe, Mitigation of wind power intermittency: Storage technology approach, Renewable and Sustainable Energy Reviews 44 (2015) 447–456. https://doi.org/https://doi.org/10.1016/j.rser.2014.12.034.

[2] M. Waterson, E. Trujillo- Baute, M. Giulietti, Intermittency and the social role of storage, Energy Policy 165 (2022) 112947. https://doi.org/https://doi.org/10.1016/j.enpol.2022.112947.

[3] K. Khan, A.K. Tareen, M. Aslam, A. Mahmood, Q. khan, Y. Zhang, Z. Ouyang, Z. Guo, H. Zhang, Going green with batteries and supercapacitor: Two dimensional materials and their nanocomposites based energy storage applications, Progress in Solid State Chemistry 58 (2020) 100254. https://doi.org/https://doi.org/10.1016/j.progsolidstchem.2019.100254.

[4] A. Muzaffar, M.B. Ahamed, C.M. Hussain, Green supercapacitors: Latest developments and perspectives in the pursuit of sustainability, Renewable and Sustainable Energy Reviews 195 (2024) 114324. https://doi.org/https://doi.org/10.1016/j.rser.2024.114324.

[5] Paris agreement, (n.d.). https://unfccc.int/process-and-meetings/the-paris-agreement (accessed September 10, 2024).

[6] M. Horn, J. MacLeod, M. Liu, J. Webb, N. Motta, Supercapacitors: A new source of power for electric cars?, Econ Anal Policy 61 (2019) 93–103. https://doi.org/10.1016/j.eap.2018.08.003.

[7] D. Iannuzzi, P. Tricoli, Metro trains equipped onboard with supercapacitors: A control technique for energy saving, SPEEDAM 2010 - International Symposium on Power Electronics, Electrical Drives, Automation and Motion (2010) 750–756. https://doi.org/10.1109/SPEEDAM.2010.5542102.

[8] Z. Lin, E. Goikolea, A. Balducci, K. Naoi, P.L. Taberna, M. Salanne, G. Yushin, P. Simon, Materials for supercapacitors: When Li-ion battery power is not enough, Materials Today 21 (2018) 419–436. https://doi.org/10.1016/j.mattod.2018.01.035.

[9] F. Wang, X. Wu, X. Yuan, Z. Liu, Y. Zhang, L. Fu, Y. Zhu, Q. Zhou, Y. Wu, W. Huang, Latest advances in supercapacitors: From new electrode materials to novel device designs, Chem Soc Rev 46 (2017) 6816–6854. https://doi.org/10.1039/c7cs00205j.

[10] Q. Wang, J. Yan, Z. Fan, Carbon materials for high volumetric performance supercapacitors: design, progress, challenges and opportunities, Energy Environ Sci 9 (2016) 729–762. https://doi.org/10.1039/C5EE03109E.

[11] J. Libich, J. Máca, J. Vondrák, O. Čech, M. Sedlaříková, Supercapacitors: Properties and applications, J Energy Storage 17 (2018) 224–227. https://doi.org/https://doi.org/10.1016/j.est.2018.03.012.

[12] M. Lu, F. Beguin, E. Frackowiak, Supercapacitors: Materials, Systems, and Applications, Wiley, 2013. https://books.google.co.in/books?id=uIt1kMzOduIC.

[13] C. Sharma, P. Vanishree, B. Rani, N. Lohia, G. Swati, R. Srivastava, S.N. Sharma, Electrochemical properties of two-dimensional hexagonal boron nitride nanosheets prepared by hydrothermal method, Electrochim Acta 463 (2023) 142848. https://doi.org/https://doi.org/10.1016/j.electacta.2023.142848.

[14] B. Rani, N.K. Sahu, Effect of aqueous electrolytes on the supercapacitive performance of glycol-mediated CoFe2O4 nanoparticles, Asia-Pacific Journal of Chemical Engineering 15 (2020) e2548. https://doi.org/https://doi.org/10.1002/apj.2548.

[15] S. Yadav, A. Devi, Recent advancements of metal oxides/Nitrogen-doped graphene nanocomposites for supercapacitor electrode materials, J Energy Storage 30 (2020) 101486. https://doi.org/https://doi.org/10.1016/j.est.2020.101486.

[16] S. Tanwar, A. Arya, A. Gaur, A.L. Sharma, Transition metal dichalcogenide (TMDs) electrodes for supercapacitors: a comprehensive review, Journal of Physics: Condensed Matter 33 (2021) 303002. https://doi.org/10.1088/1361-648x/abfb3c.

[17] M.R. Benzigar, V.D.B.C. Dasireddy, X. Guan, T. Wu, G. Liu, Advances on Emerging Materials for Flexible Supercapacitors: Current Trends and Beyond, Adv Funct Mater 30 (2020). https://doi.org/10.1002/adfm.202002993.

[18] Y.-N. Wu, W.A. Saidi, P. Ohodnicki, B. Chorpening, Y. Duan, First-Principles Investigations of the Temperature Dependence of Electronic Structure and Optical Properties of Rutile TiO_2, 122 (2018). https://doi.org/10.1021/acs.jpcc.8b06941.

[19] A.K. Yadav, S. N S, R. Singh, P.P. Das, V. Garg, S.K. Pandey, DFT Calculations for Temperature Stable Quantum Capacitance of VS2 Based Electrodes for Supercapacitors, IEEE Trans Nanotechnol 23 (2024) 132–138. https://doi.org/10.1109/TNANO.2024.3358017.

[20] Bharti, G. Ahmed, Y. Kumar, S. Sharma, DFT computation of quantum capacitance of pure and doped niobium nitrides for supercapacitor applications, Ceram Int 47 (2021) 18948–18955. https://doi.org/https://doi.org/10.1016/j.ceramint.2021.03.237.

[21] P. Kreczanik, P. Venet, A. Hijazi, G. Clerc, Study of supercapacitor aging and lifetime estimation according to voltage, temperature, and RMS current, IEEE Transactions on Industrial Electronics 61 (2014) 4895–4902. https://doi.org/10.1109/TIE.2013.2293695.

[22] H. Yang, Dependence of Supercapacitor Peukert Constant on Voltage, Aging, and Temperature, IEEE Trans Power Electron (2019) 1–1. https://doi.org/10.1109/tpel.2018.2890392.

[23] B. Purty, R.B. Choudhary, A. Biswas, G. Udayabhanu, Temperature dependent supercapacitive performance of NH 3 modified TiO 2 decorated PPy nanohybrids in various electrolyte systems, Synth Met 249 (2019) 1–13. https://doi.org/10.1016/j.synthmet.2019.01.012.

[24] H. Ahmad, W.Y. Wan, D. Isa, Modeling the Ageing Effect of Cycling Using a Supercapacitor-Module Under High Temperature With Electrochemical Impedance Spectroscopy Test, IEEE Trans Reliab 68 (2019) 109–121. https://doi.org/10.1109/TR.2018.2869212.

[25] S. Jha, M. Yen, Y.S. Salinas, E. Palmer, J. Villafuerte, H. Liang, Machine learning-assisted materials development and device management in batteries and supercapacitors: performance comparison and challenges, J. Mater. Chem. A 11 (2023) 3904–3936. https://doi.org/10.1039/D2TA07148G.

[26] S. Mishra, R. Srivastava, A. Muhammad, A. Amit, E. Chiavazzo, M. Fasano, P. Asinari, The impact of physicochemical features of carbon electrodes on the capacitive performance of supercapacitors: a machine learning approach, Sci Rep 13 (2023) 6494. https://doi.org/10.1038/s41598-023-33524-1.

[27] T. Wang, R. Pan, M.L. Martins, J. Cui, Z. Huang, B.P. Thapaliya, C.-L. Do-Thanh, M. Zhou, J. Fan, Z. Yang, M. Chi, T. Kobayashi, J. Wu, E. Mamontov, S. Dai, Machine-learning-assisted material discovery of oxygen-rich highly porous carbon active materials for aqueous supercapacitors, Nat Commun 14 (2023) 4607. https://doi.org/10.1038/s41467-023-40282-1.

[28] N. Wagner, J.M. Rondinelli, Theory-guided machine learning in materials science, Front Mater 3 (2016). https://doi.org/10.3389/fmats.2016.00028.

[29] J.F. Rodrigues, L. Florea, M.C.F. de Oliveira, D. Diamond, O.N. Oliveira, Big data and machine learning for materials science, Discov Mater 1 (2021) 12. https://doi.org/10.1007/s43939-021-00012-0.

[30] R. Ramprasad, R. Batra, G. Pilania, A. Mannodi-Kanakkithodi, C. Kim, Machine learning in materials informatics: recent applications and prospects, NPJ Comput Mater 3 (2017) 54. https://doi.org/10.1038/s41524-017-0056-5.

[31] T. Gao, W. Lu, Machine learning toward advanced energy storage devices and systems, IScience 24 (2021) 101936. https://doi.org/https://doi.org/10.1016/j.isci.2020.101936.

[32] M.-F. Ng, J. Zhao, Q. Yan, G.J. Conduit, Z.W. Seh, Predicting the state of charge and health of batteries using data-driven machine learning, Nat Mach Intell 2 (2020) 161–170. https://doi.org/10.1038/s42256-020-0156-7.

[33] W.Z. Tawfik, S.N. Mohammad, K.H. Rahouma, G.M. Salama, E. Tammam, Machine learning models for capacitance prediction of porous carbon-based supercapacitor electrodes, Phys Scr 99 (2024) 26001. https://doi.org/10.1088/1402-4896/ad190c.

[34] H. Su, S. Lin, S. Deng, C. Lian, Y. Shang, H. Liu, Predicting the capacitance of carbon-based electric double layer capacitors by machine learning, Nanoscale Adv 1 (2019) 2162–2166. https://doi.org/10.1039/C9NA00105K.

[35] M.A. Ebied, M. A.Azim, A. Emad-Eldeen, AI-based approach for predicting the storage performance of zinc oxide-based supercapacitor electrodes, J Energy Storage 94 (2024) 112292. https://doi.org/https://doi.org/10.1016/j.est.2024.112292.

[36] M.L. Adam, O.A. Moses, J.P. Mailoa, C.-Y. Hsieh, X.-F. Yu, H. Li, H. Zhao, Navigating materials chemical space to discover new battery electrodes using machine learning, Energy Storage Mater 65 (2024) 103090. https://doi.org/https://doi.org/10.1016/j.ensm.2023.103090.

[37] A. Keddouda, R. Ihaddadene, A. Boukhari, A. Atia, M. Arıcı, N. Lebbihiat, N. Ihaddadene, Photovoltaic module temperature prediction using various machine learning algorithms: Performance evaluation, Appl Energy 363 (2024) 123064. https://doi.org/https://doi.org/10.1016/j.apenergy.2024.123064.

[38] J. Vivian, E. Prataviera, N. Gastaldello, A. Zarrella, A comparison between grey-box models and neural networks for indoor air temperature prediction in buildings, Journal of Building Engineering 84 (2024) 108583. https://doi.org/https://doi.org/10.1016/j.jobe.2024.108583.

[39] V.L. Deringer, Modelling and understanding battery materials with machine-learning-driven atomistic simulations, Journal of Physics: Energy 2 (2020) 041003. https://doi.org/10.1088/2515-7655/abb011.

[40] J.A. Keith, V. Vassilev-Galindo, B. Cheng, S. Chmiela, M. Gastegger, K.-R. Müller, A. Tkatchenko, Combining Machine Learning and Computational Chemistry for Predictive Insights Into Chemical Systems, Chem Rev 121 (2021) 9816–9872. https://doi.org/10.1021/acs.chemrev.1c00107.

[41] B. Meredig, A. Agrawal, S. Kirklin, J.E. Saal, J.W. Doak, A. Thompson, K. Zhang, A. Choudhary, C. Wolverton, Combinatorial screening for new materials in unconstrained composition space with machine learning, Phys Rev B 89 (2014) 94104. https://doi.org/10.1103/PhysRevB.89.094104.

[42] S. Ghosh, G.R. Rao, T. Thomas, Machine learning-based prediction of supercapacitor performance for a novel electrode material: Cerium oxynitride, Energy Storage Mater 40 (2021) 426–438. https://doi.org/https://doi.org/10.1016/j.ensm.2021.05.024.

[43] U.N. Kumar, S. Ghosh, C.R. Jeevandoss, T. Thomas, Temperature dependent performance analysis of all-oxynitride asymmetric solid-state supercapacitor, J Energy Storage 74 (2023) 109563. https://doi.org/https://doi.org/10.1016/j.est.2023.109563.

[44] G. Kresse, D. Joubert, From ultrasoft pseudopotentials to the projector augmented-wave method, Phys Rev B 59 (1999) 1758–1775. https://doi.org/10.1103/PhysRevB.59.1758.

[45] P.E. Blöchl, Projector augmented-wave method, Phys Rev B 50 (1994) 17953–17979. https://doi.org/10.1103/PhysRevB.50.17953.

[46] J.P. Perdew, K. Burke, M. Ernzerhof, Generalized Gradient Approximation Made Simple [Phys. Rev. Lett. 77, 3865 (1996)], Phys Rev Lett 78 (1997) 1396. https://doi.org/10.1103/PhysRevLett.78.1396.

[47] H.J. Monkhorst, J.D. Pack, Special points for Brillouin-zone integrations, Phys Rev B 13 (1976) 5188–5192. https://doi.org/10.1103/PhysRevB.13.5188.

[48] C. Zhao, X. Lu, H. Tu, Y. Yang, S. Wang, A. Chen, H. Zhang, Research on specific capacitance prediction of biomass carbon-based supercapacitors based on machine learning, J Energy Storage 97 (2024) 112974. https://doi.org/https://doi.org/10.1016/j.est.2024.112974.

[49] T.A. Alrebdi, Y.S. Wudil, U.F. Ahmad, F.A. Yakasai, J. Mohammed, F.H. Kallas, Predicting the thermal conductivity of Bi2Te3-based thermoelectric energy materials: A machine learning approach, International Journal of Thermal Sciences 181 (2022) 107784. https://doi.org/https://doi.org/10.1016/j.ijthermalsci.2022.107784.

[50] S. Wang, K. Huang, C. Lian, H. Liu, 15 - Machine learning and data-driven material exploration for supercapacitors, in: S.G. Krishnan, H.D. Pham, D.P. Dubal (Eds.), Supercapacitors, Elsevier, 2024: pp. 353–370. https://doi.org/https://doi.org/10.1016/B978-0-443-15478-2.00015-2.

[51] M. Aria, C. Cuccurullo, A. Gnasso, A comparison among interpretative proposals for Random Forests, Machine Learning with Applications 6 (2021) 100094. https://doi.org/https://doi.org/10.1016/j.mlwa.2021.100094.

[52] A. Fuertes, Metal oxynitrides as emerging materials with photocatalytic and electronic properties, Mater Horiz 2 (2015) 453–461. https://doi.org/10.1039/c5mh00046g.

[53] M. Woźny, J. Cebulski, A. Marcelli, M. Piccinini, E.M. Sheregii, Influence of the electron-phonon interaction on the temperature dependence of the phonon mode frequency in the II-VI compound solid solutions, J Appl Phys 117 (2015) 025702. https://doi.org/10.1063/1.4905293.

[54] Y. Cho, A. Yamaguchi, R. Uehara, S. Yasuhara, T. Hoshina, M. Miyauchi, Temperature dependence on bandgap of semiconductor photocatalysts, J Chem Phys 152 (2020) 231101. https://doi.org/10.1063/5.0012330.

[55] G. Lucovsky, Electronic Structure, Amorphous Morphology And Thermal Stability Of Transition Metal Oxide And Chalcogenide Alloys, 2001.

[56] S. Zollner, M. Cardona, S. Gopalan, Isotope and temperature shifts of direct and indirect band gaps in diamond-type semiconductors, Phys Rev B 45 (1992) 3376–3385. https://doi.org/10.1103/PhysRevB.45.3376.

[57] F. Giustino, M.L. Cohen, S.G. Louie, Electron-phonon interaction using Wannier functions, Phys Rev B 76 (2007) 165108. https://doi.org/10.1103/PhysRevB.76.165108.

[58] C. Costentin, J.-M. Savéant, Energy storage: pseudocapacitance in prospect, Chem Sci 10 (2019) 5656–5666. https://doi.org/10.1039/C9SC01662G.

[59] Y. Jiang, J. Liu, Definitions of Pseudocapacitive Materials: A Brief Review, ENERGY & ENVIRONMENTAL MATERIALS 2 (2019) 30–37. https://doi.org/https://doi.org/10.1002/eem2.12028.

[60] Y. Shi, M. Zhang, D. Yang, J. Li, Study on preparation of high performance manganese dioxide supercapacitor by cyclic voltammetry, Ionics (Kiel) 27 (2021) 4521–4529. https://doi.org/10.1007/s11581-021-04223-6.

[61] Y. Lin, C. Lian, M.U. Berrueta, H. Liu, R. van Roij, Microscopic Model for Cyclic Voltammetry of Porous Electrodes, Phys Rev Lett 128 (2022) 206001. https://doi.org/10.1103/PhysRevLett.128.206001.

[62] F. Yu, T. Huang, P. Zhang, Y. Tao, F.-Z. Cui, Q. Xie, S. Yao, F. Wang, Design and synthesis of electrode materials with both battery-type and capacitive charge storage, Energy Storage Mater 22 (2019) 235–255. https://doi.org/https://doi.org/10.1016/j.ensm.2019.07.023.

[63] R. Kumar, M. Bag, Quantifying Capacitive and Diffusion-Controlled Charge Storage from 3D Bulk to 2D Layered Halide Perovskite-Based Porous Electrodes for Efficient Supercapacitor Applications, The Journal of Physical Chemistry C 125 (2021) 16946–16954. https://doi.org/10.1021/acs.jpcc.1c05493.

[64] G. Song, X. Huang, H. Feng, Z. Zuo, J. Li, D. Tang, Q. Wei, B.-A. Mei, Physical interpretations of diffusion-controlled intercalation and surface-redox charge storage behaviors, Energy Storage Mater 61 (2023) 102859. https://doi.org/https://doi.org/10.1016/j.ensm.2023.102859.

[65] R. Nariswari, H. Pudjihastuti, Support Vector Machine Method for Predicting Non-Linear Data, Procedia Comput Sci 227 (2023) 884–891. https://doi.org/https://doi.org/10.1016/j.procs.2023.10.595.

[66] S.M. LaValle, M.S. Branicky, S.R. Lindemann, On the relationship between classical grid search and probabilistic roadmaps, Int J Rob Res 23 (2004) 673–692.

[67] W. Zhou, Z. Liu, W. Chen, X. Sun, M. Luo, X. Zhang, C. Li, Y. An, S. Song, K. Wang, X. Zhang, A Review on Thermal Behaviors and Thermal Management Systems for Supercapacitors, Batteries 9 (2023). https://doi.org/10.3390/batteries9020128.

[68] Y. Wang, H. Dong, K. Ma, H. Wang, J. Zhang, Multi frequency stability optimization of integrated energy systems considering virtual energy storage characteristics of heating networks, Appl Therm Eng 257 (2024) 124254. https://doi.org/https://doi.org/10.1016/j.applthermaleng.2024.124254.

[69] J.F. Pedrayes, M.G. Melero, J.M. Cano, J.G. Norniella, G.A. Orcajo, M.F. Cabanas, C.H. Rojas, Optimization of supercapacitor sizing for high-fluctuating power applications by means of an internal-voltage-based method, Energy 183 (2019) 504–513. https://doi.org/https://doi.org/10.1016/j.energy.2019.06.145.